Research Signpost
Trivandrum
Kerala, India

Recent Advances in Pharmaceutical Sciences VIII, 2018: 1-18 ISBN: 978-81-308-0579-5
Editors: Diego Muñoz-Torrero, Yolanda Cajal and Joan Maria Llobet

1. Magnetic nanoparticles: From diagnosis to therapy

M. Antònia Busquets and Joan Estelrich
Department of Pharmacy, Pharmaceutical Technology and Physical Chemistry
Institute of Nanoscience and Nanotechnology, IN2UB
Faculty of Pharmacy and Food Sciences, University of Barcelona
Avda Joan XXIII, 27-31, 08028 Barcelona

Abstract. Magnetic nanoparticles have proven to be promising theranostic agents, namely tools for therapy and diagnosis. Among them, superparamagnetic iron oxide nanoparticles (SPIONs) highlight for their biocompatibility and reduced toxicity. Here, we describe the synthesis and characterization of SPIONs by co-precipitation of ferric and ferrous salts under mild conditions. These particles were able to accumulate in inflamed areas fact that was increased upon the application of an external magnetic field. Resonance magnetic imaging studies have shown their suitability as negative contrast agents for diagnosis. In addition, hybrid nanoparticles were obtained by incorporating the above described SPIONs into liposomes or nanoemulsions. The findings have confirmed the high potential of these systems for biomedical applications.

Introduction

The impact of nanotechnology is strongly associated to the development of nanomaterials and nanoparticles (NPs) [1,2]. In particular, magnetic nanoparticles (MNs) present a number of advantages if compared to other

Correspondence/Reprint request: Dr. M. Antònia Busquets, Department of Pharmacy, Pharmaceutical Technology and Physical Chemistry, Faculty of Pharmacy and Food Sciences, University of Barcelona, Avda Joan XXIII, 27-31, 08028 Barcelona. E-mail: mabusquetsvinas@ub.edu

nanosystems. Their magnetic properties can be exploited for the targeting of drugs and as contrast agents. The duality that involves both therapy and diagnosis, all in one, or theranostic effect [3] has gained interest in the biomedical field, becoming an encouraging approach towards a personalized medicine. For that purpose, the design of nanosystems often requires the combination of one or several modifications of traditional NPs. It usually involves changes in their surface or their incorporation into other NPs conferring in this way also versatile, multifunctional, biocompatible and biodegradable properties [4,5].

There is a great variety of materials that show magnetism in some extent depending on their atomic structure and temperature. The compounds with stable magnetic properties are classified into two main groups: ferromagnets, with permanent magnetism, and paramagnets, with magnetism that appears upon the application of an external magnetic field [6]. On the other hand, the size is a decisive aspect concerning to the functionality of the MNs. A ferromagnet of macroscopic size contains numerous regions called magnetic domains in the demagnetized state. Within each domain all the atomic moments (represented as arrows in Fig 1) are aligned in one of the directions leading to spontaneous magnetization.

The direction of the magnetization, however, varies from domain to domain so as to minimize the magnetostatic energy. On a purely statistical basis, all available easy directions will be used equally in the material. Hence the particle as a whole will only show a net magnetization when submitted to an applied field [7]. A ferromagnet below a certain critical diameter (D_{CR}) shows a single domain. Further reduction in size results in a superparamagnetic (D_{SPM}) behavior meaning that magnetic properties are only present upon the application of an external magnetic field.

Among the several types of MNs, up to now, iron oxide nanoparticles (IONs) have proven to be the most promising MNs for theranostic applications mainly for their high imaging sensitivity, therapeutic efficacy, inherent biocompatibility and low cost [8]. This group comprises different chemical combinations of iron such as ferrites with a general formula MFe_2O_4 (M= Co, Ni, Zn, Mn), magnetite (Fe_3O_4), maghemite (γ-Fe_2O_3) or the non-stoichiometric mixture of the last two, with diameters comprised between 1 and 100 nm. This array of sizes supposes an additional advantage in the design of IONs with different magnetic behavior and consequently for a variety of applications. Therefore, below a certain diameter, D_{SPM}, they are superparamagnetic being magnetized only in presence of a magnetic field. Superparamagnetic IONs (SPIONs) can be directed by an external magnet

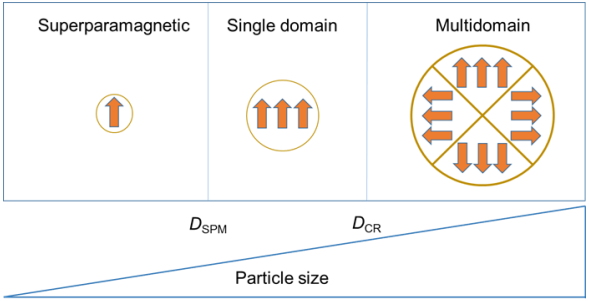

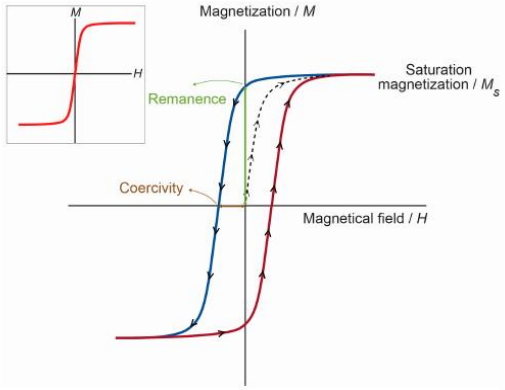

Figure 1. Left) Magnetic regimes of ferromagnetic materials classified according to their size. Right) Changes of magnetization (*M*) for a ferromagnetic material depending on the application of an external magnetic field (*H*). The arrows on the cycle indicate the direction in the increase or decrease of the field amplitude. The inset shows the behavior of a superparamagnetic material submitted to the same external magnetic field [6].

towards a given target zone (Figure 2). Then, the application of a magnetic field moves the SPIONs toward the magnet and concentrates near its location. SPIONs revert to a non-magnetic state upon removal of the external magnet [9].

The application of a high-frequency alternating magnetic field can selectively heat SPIONs resulting in a hyperthermia effect that can be exploited for drug targeting. Therefore, their responsiveness to a magnetic field makes these particles suitable stimuli-sensitive systems as they can change their physical properties in response to an external stimulus and, in case of carrying drugs, these can be selectively delivered to the target site, minimizing any side effects [10].

The magnetic properties SPIONs make them suitable candidates for molecular imaging (MI), a diagnostic approach that combines molecular biology and in vivo imaging performed in real time with the possibility of sequential and longitudinal monitoring. MI has the advantage over other diagnostic tools that allows high soft tissue contrast, spatial resolution and penetration depth for what it is considered one of the most powerful noninvasive imaging techniques in diagnostic [11,12,13]. In particular, SPIONs have shown interesting results as negative contrast agents in magnetic

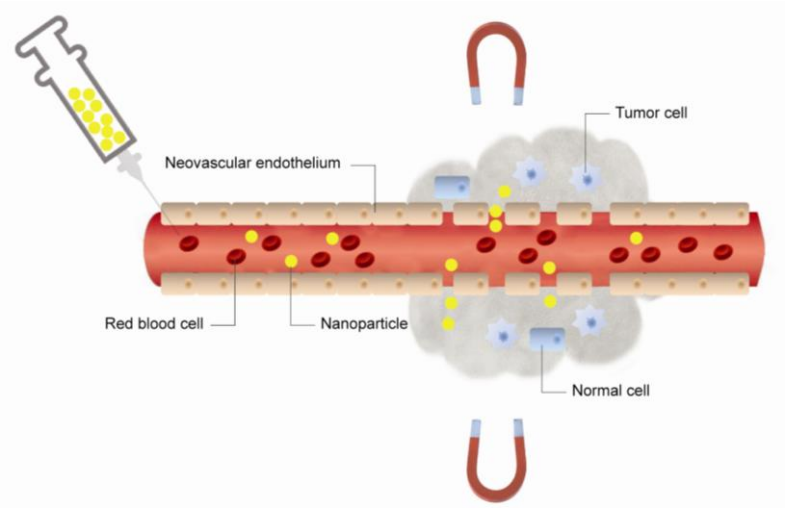

Figure 2. Procedure for magnetically-guided drug targeting of nanoparticles. The enhanced permeability and retention effect facilitates the extravasation of the nanoparticles from the pores in leaky tumor blood vessel walls [6].

resonance imaging (MRI) [14,15]. SPIONs improved the contrast-to-noise ratio in MRI by shortening the spin-spin T_2 relaxation times of the water protons within the tissues or regions of interest, enhancing in this way the image contrast.

The versatility and functionality of SPIONs can be enhanced by modifications of their surface consisting mainly on coating the surface with ligands or by their inclusion into other nanoparticles giving hybrid nanosystems such as liposomes or nanoemulsions [16,17]. The combination of liposomes and SPIONs results in multifunctional magnetoliposomes (MLs) or *all in one* system that can also incorporate a variety of molecules. The first reference on MLs is found in a 1989 publication by Kiwada [18]. These MLs had a size in the micrometer range, far too big for biological applications. From then, several procedures have been described resulting in nanometer-sized MLs [19,20]. Figure 3 shows a prototype of multifunctional or hybrid liposome (large unilamellar liposome, LUV), composed of phospholipids, with theranostic properties. Thus, encapsulated SPIONs in the inner core or embedded into the lipid bilayer provide a tool for magnetic targeting; the presence of a peptide such as the cyclic arginine-aspartic acid-glutamine motif, allows

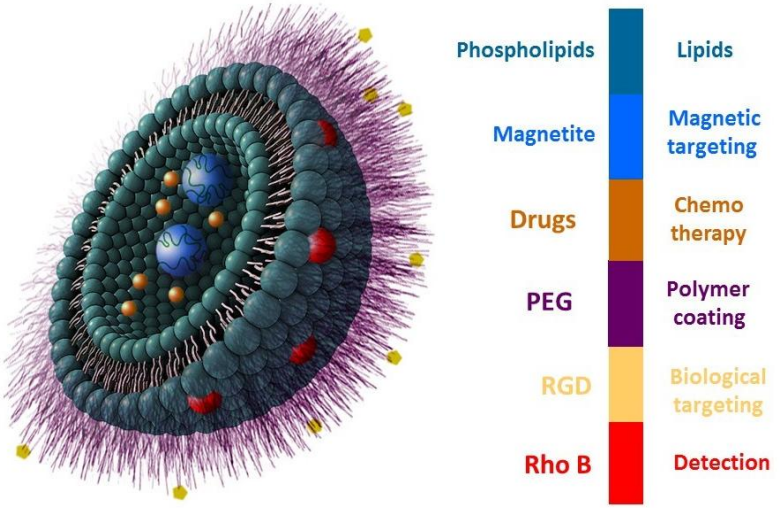

Figure 3. Prototype of a multifunctional large unilamellar magnetoliposome with the associated properties provided by each component. PEG: Polyethylene glycol; RGD: Arginine (R)-Glycine (G)-Aspartic acid (D); Rho-B: Lissamine Rhodamine B

for biological targeting; drugs located depending on their hydrophilic or hydrophobic character as SPIONs in the aqueous compartment or among the lipid acyl-chains, respectively, make the systems appropriate for chemotherapy. On another hand, the presence of polymers (e.g. polyethylene glycol, PEG) on the outer leaflet of the vesicles, protect them from the opsonization and rapid uptake from the bloodstream once administered. Finally, fluorescent probes can be incorporated to the lipid bilayer for detection purposes.

Similarly, the incorporation of SPIONs into oil-in-water nanoemulsions results in magnetic nanoemulsions (MNEs). MNEs can include the same components as mentioned for liposomes and are particularly interesting as drug delivery systems of hydrophobic drugs. Both, MNEs and MLs are biodegradable and show low toxicity [22].

1. Synthesis and characterization of iron oxide nanoparticles

SPIONs were synthesized according to the method described by Berger et al. [22]. Briefly, a mixture of Fe $(OH)_2$ and Fe $(OH)_3$ was obtained after the stoichiometric reaction of Fe^{2+} and Fe^{3+} in presence of strong alkali and under vigorous stirring. Subsequent fast aging of those hydroxides generates magnetite. The overall reaction is:

$$2FeCl_3 + FeCl_2 + 4H_2O + 8NH_3 \rightarrow Fe_3O_4 + 8NH_4^+ + 8Cl^-$$

In order to provide colloidal stability to the particles and prevent their aggregation, they are usually coated with other nanoscale materials, resulting in the so named ferrofluids. Hydrophilic polymers such as dextran and its

Table 1. Physicochemical parameters of ALG or CHI coated NPs.

Coating	Size[1]/ nm	PDI[2]	Magnetization/ emu g^{-1}	ζ potential/ mV
ALG	50 ± 5	0.15± 0.02	56.8±0.2	-34±1
CHI	100 ± 7	0.18± 0.01	59.3±1.0	25±1

[1] Hydrodynamic diameter measured by dynamic light scattering
[2] Polydispersity index. Its value varies from 0 for a monodisperse sample to 1 for a polydisperse population.

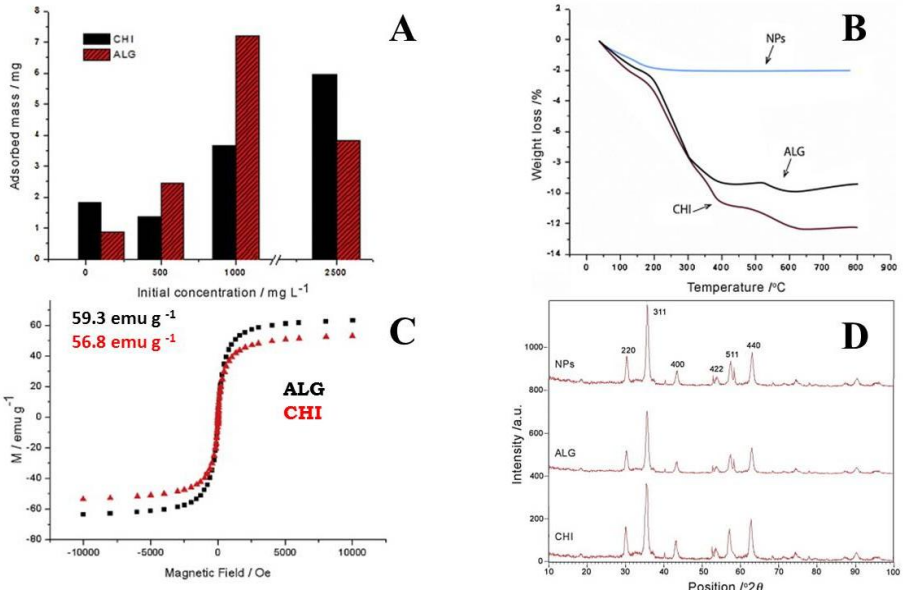

Figure 4. Physicochemical characteristics of SPIONs coated with CHI or ALG. A) Mass of polymer adsorbed at 300 K depending on the initial amount of polymer; B) thermogravimetric analysis of the coated (CHI, ALG) and uncoated NPs, C) magnetic behavior and, D) XRD paterns [23].

derivatives, polyethylene glycol (PEG), chitosan (CHI) and alginate (ALG) are among the most used for the stabilization of naked magnetic nanoparticles [23]. We have studied the influence of the initial amount of CHI, ALG and PEG of different molecular weights in the stabilization of the magnetite. The optimal concentration of polymer needed for coating the NPs was calculated through adsorption isotherms and the amount coated was measured by thermogravimetry.

The ferrofluids were also characterized by measuring their size and size distribution by dynamic light scattering (DLS) and charge (ζ potential) with a Zetasizer Nano ZS90 (Malvern Instruments, UK). High-resolution TEM (HR-TEM, 2010F Jeol Microscope, Japan) indicated that the particle diameter was around 11 nm, value that was confirmed by X ray diffraction (XRD). Some of the above results are illustrated in Table 1 and Figure 4.

The magnetic properties of the ferrofluids under the influence of a magnetic field were measured with a superconducting quantum interference device (SQUID) magnetometer (Quantum design MPMS XL, San Diego, California, USA) at room temperature. All samples showed superparamagnetism without magnetic hysteresis at room temperature.

2. Synthesis and characterization of hybrid nanoparticles

2.1. Magnetoliposomes

A lipid or lipid mixture of interest in chloroform/methanol (2:1, v/v) was introduced into a round bottom flask and the organic solvent was evaporated in a rotavapor under reduced pressure until the formation of a thin film. The dried mixture was then hydrated with an aqueous suspension of hydrophilic magnetic particles. In the case of hydrophobic SPIONs and hydrophobic drugs as indomethacin, they were added to the organic mixture and proceed as mentioned before. Up to now, the samples consist on a heterogeneous population of MLs. In order to obtain homogeneous samples, MLs were sonicated in an ultrasonic processor (Hielscher, Teltow, Germany) or submitted to extrusion cycles through a 200 nm polycarbonate filters (Extrude device, Avestin, Ottawa, Canada). Ligand-targeted MLs with the arginine-glycine-aspartic acid motif (RGD) were also designed to study their ability to interact with cancer cells [24]. MLs were characterized as mentioned for SPIONs and additionally, the amount of lipid, encapsulated drug and SPIONs were measured as described in [9]. The average size of MLs was around 200 nm with low polydispersity (< 0.2).

2.2. Magnetic nanoemulsions

The advantage of MNEs over MLs is their higher loading capacity of hydrophobic materials. Oil in water MNEs were prepared by mixing olive oil, cholesterol (CHOL) and the phospholipids 1,2-distearoyl-*sn*-glycero-3-phosphoethanolamine (DSPE-PEG) and 1,2-distearoyl-*sn*-glycero-3-phosphocholine (DSPC) dissolved in organic solvent. Hydrophobic SPIONs and indomethacin were also added to the organic phase. Then, the organic solvent was removed by rotary evaporation at 35 ^{o}C and the dried mixture was hydrated with water or buffered saline solution. The resulting crude emulsion was homogenized by spontaneous emulsification (low energy) or ultrasonication with an UP200 St ultrasonic processor (Hielscher, Teltow, Germany) (high energy) (Figure 5) [26,27]. NEs were characterized as described for MLs.

For internalization studies in cells, MLs and MNEs were labeled with the fluorescent probe 1,2-dimyristoyl-sn-glycero-3-phosphoethanolamine-N-(lissamine rhodamine B sulfonyl) (ammonium salt) (Rho-PE). In both hybrid nanosystems, SPIONs kept their original superparamagnetic properties.

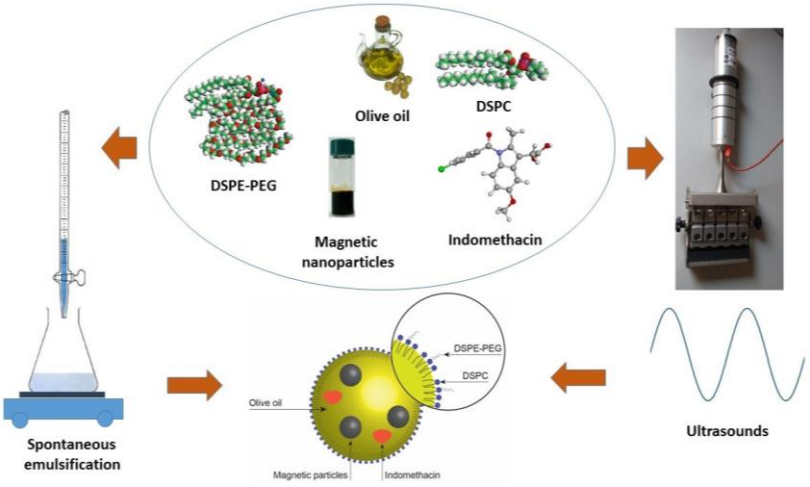

Figure 5. Schematic representation of the magnetic NEs loading indomethacin and SPIONs obtained by high energy method (ultrasounds) or low energy method (spontaneous emulsification). On top components of the NEs [27].

3. Magnetoliposomes accumulate in inflamed sites

The ability of MLs to reach inflamed areas was studied in a first assay by administering intravenously bare MLs to mice, namely MLs containing only phospholipids with encapsulated SPIONs [25]. Previously, sterile air pouches were produced by injecting air subcutaneously into the back of the mice. Then, animals were divided in four groups. In two of them, acute inflammation was induced by injecting 1.2 % carrageenan (phologen) to the pouch (inflammation groups). The injection in the other two groups (control groups) consisted on sterile saline. MLs were then injected i.v. to one of the two inflammation (I + MLs), and control groups (C + MLs). Mice were sacrificed 20 min after the injection.

The iron content in exudates (pouch), plasma and organs was analyzed by inductively coupled plasma atomic emission spectroscopy (ICP-AES, Perkin Elmer Optima 3200RL, Massachusetts, USA). Iron levels were higher in animals with inflammation that in control animals. After the administration of MLs to the control group, iron content increased similarly to the measured for animals with inflammation and MLs. There was no change in the concentration of iron in the liver after i.v. administration, whereas there was an increase in the spleen compared to the control group (Figure 6).

Iron biodistribution indicated that MLs accumulated mainly in the inflammation zone without the need of an external magnet to potentiate the migration of MLs to the target site. A possible explanation to this fact is the enhanced permeability and retention effect as a consequence of the leaky vasculature of the tumor or in inflamed areas that allows the intratumoral accumulation of particles smaller than 200 nm [28].

In a later study [9], a similar experiment was performed in which an external magnetic field induced a selective biodistribution of bare MLs to the inflamed area (Figure 7).

By this magnetically guided drug targeting approach, MLs accumulated at the site of inflammation (exudates) and simultaneously were removed from the blood. In addition, their content decreased in the liver and spleen. The increase in iron levels in exudates depended on the time of exposure of the external magnetic field (Table 2).

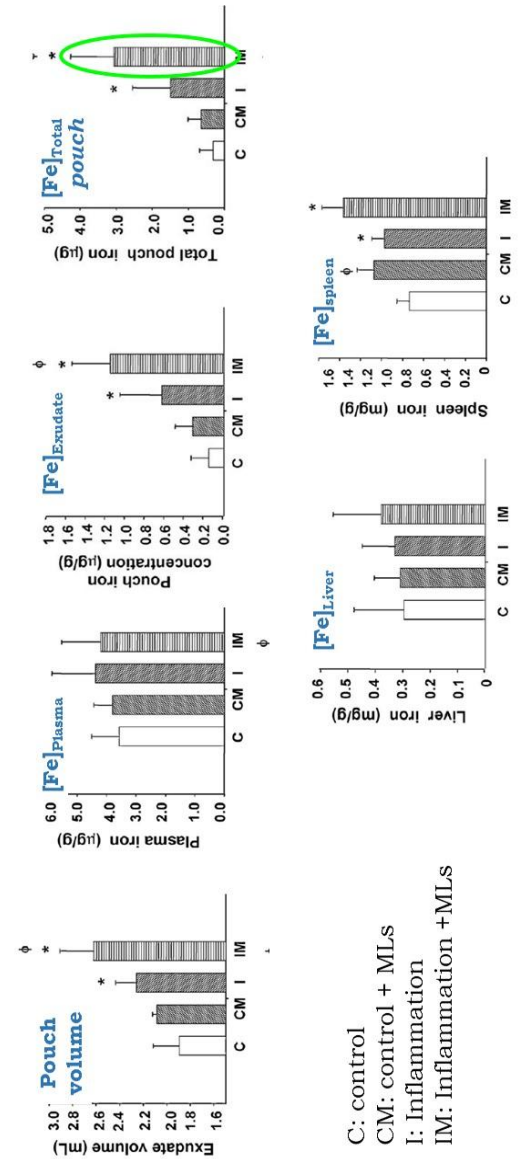

Figure 6. Pouch volume and iron concentration in plasma, pouch, liver and spleen 20 min after sterile saline (control and inflammation groups) or MLs (control and inflammation groups) i.v. injection. In these experiments inorganic iron can not be distinguished from endogenous iron. Total iron content in the pouch for the group IM (green circle) was significantly higher than in the other groups confirming the accumulation of SPIONs [25].

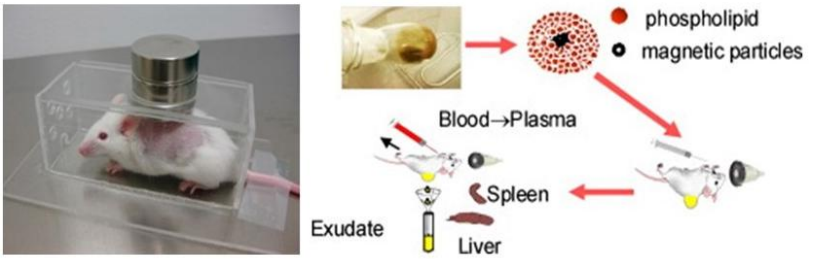

Figure 7. Experimental device to measure the effect of an external magnetic field on the biodistribution of MLs (left) after i.v. injection into mice (right). An inflammatory focus was introduced on their backs. Two $ND_2Fe_{12}B$ disk magnets (25 x 10 mm, of 600 mT per side were place over the hole in the Plexiglas cages [9].

Table 2. Iron concentration ($\mu g \cdot g^{-1}$) in exudates, plasma, liver and spleen.

Groups	Exudates	Plasma	Liver	Spleen
C	0.04 ± 0.04	4.04± 1.02	621±310	665±180
I	0.26 ± 0.13	4.01± 1.27	712±224	836±278
IN	0.33 ± 0.11	4.12± 1.07	873±99	1,446±390
INM	0.56 ± 0.12	2.89± 0.42	674±64	1,264±35

C: control, mice with back air pouch receiving sterile saline; I: inflammation control group, animals with carrageenan-induced inflammation in the air pouch receiving saline; IN: as I but receiving MLs i.v; and INM as IN but under the effect of a magnet located just above the inflammatory pouch for 20 min (Figure 7) [9].

TEM micrograph of the exudates showed the presence of intact MLs 20 min after the injection. This is a consequence of the size of the SPIONs (~ 12 nm) that is too large to passively cross the phospholipid bilayer. Iron release is only possible after the action of opsonins and cells of the mononuclear phagocyte system or other destabilizing agents.

4. Ligand-targeted Magnetoliposomes

It is described that nanoparticles can be directed to a target site by functionalization of the external core. Insertion of peptides is one of the most

successful strategies [29]. For instance, the cyclic RGD peptide, bounded to the outer leaflet of the liposomal bilayer thorough a lipid-PEG-maleimido group, can bind vascular endothelial cells at inflammation sites [30]. Dubey et al. [31] indicated that cyclic RGD peptide anchored sterically stabilized liposomes bearing 5-FU were significantly more active against primary tumor and metastasis than the non-targeted sterically stabilized liposomes and free drug. Therefore cyclic RGD peptide anchored sterically stabilized liposomes hold potential of targeted cancer chemotherapeutics. Based on this premise, we designed an experiment aimed to study the targeting of RGD-MLs to integrin $\alpha_V\beta_3$ expressed in many cancer cells as the Hela cellular line. Bare MLs and PEG-sterically stabilized MLs were used as control (Figure 8).

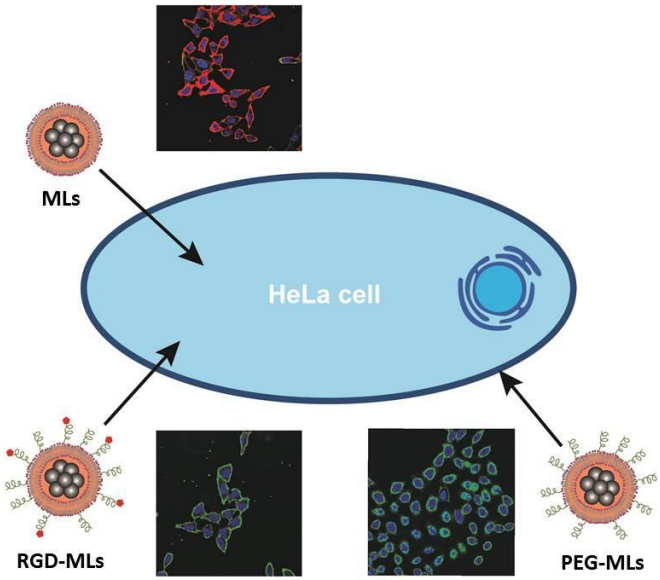

Figure 8. Magnetoliposomes, MLs, composed of phosphatidylcholine (PC)/cholesterol (CHOL) (8:2 mol/mol) synthesized for internalization studies in Hela and 3T3 cells. PEG-MLs: pegilated MLs (long circulating) and RGD-MLs: functionalized MLs (biological targeting). The images correspond to confocal observations (Leika TCS-SP2, Heidelberg, Germany) after the incubation of MLs with Hela cells for 4 h. MLs were labeled with rhodamine-PE (red), the nucleus with membrane-permeable dye Hoeschst 33342 (blue) and the cell membrane with cell membrane-impermeable Alexa Fluor 488-conjugated wheat germ agglutinin (green).

Previously to the cellular internalization studies, the cytotoxicity of naked SPIONs and MLs was analyzed in Hela and 3T3 (control) cellular lines by two typical assays, MTT that measures the metabolic activity in the mitochondria of viable cells and NR that gives information about the membrane integrity. MLs were viable at the concentrations studied [24].

Unexpectedly, confocal microscopy and flow cytometry showed that bare MLs were internalized in higher extent than the MLs displaying the targeting moiety [24]. Apparently, cellular uptake of ligand-targeted MLs was inhibited by the PEG chains of the surface. To overcome this drawback, MLs surface should display PEG chains of different length, short to prevent the adsorption of proteins on the surface of the proteins and a long chain to favor the interaction with the cellular receptor.

5. Magnetoliposomes as contrast agents for Magnetic Resonance Imaging

Agar phantoms with MLs or SPIONs were prepared to avoid particle aggregation during the application of the magnetic field. Then MRI measurements were performed on a 7.0 T BioSpec 70/30 horizontal animal scanner (Bruker BioSpin, Ettlingen, Germany). T_1 (positive contrast) and T_2 (negative contrast) relaxometry maps as well as the relaxation rates r_1 ($1/T_1$) and r_2 ($1/T_2$) were obtained as described in [14]. The relaxivity for a MRI contrast agent calculated from equation 1 is described as the increase of the relaxation rate of the water (solvent) induced by 1 mmol.L^{-1} of the active ion.

$$r_{i,obs} = \left[\frac{1}{T_{i,obs}} - \frac{1}{T_{i,water}}\right] / C_{CA} \qquad \text{Equation 1}$$

where i refers to 1 (r_1) or 2 (r_2), and C_{CA}, to the iron concentration of the contrast agent (SPIONs).

Table 3 shows the relaxivity values for the SPIONs alone and incorporated into liposomes of different composition. r_1 is poorly sensitive to SPIONs at 7 T due to the reduced susceptibility to dipolar contributions at high field, in addition to the presence of bulky surface groups hindering the surface accessibility of water to the magnetic cores. Contrarily, r_2 values are bigger because transversal relaxivities are highly sensitive to the presence of substances around the magnetic core.

Table 3. r_1, r_2 and r_2/r_1 ratio of magnetic hydrophobic (O) and hydrophilic (H) nanoparticles alone or encapsulated in liposomes of different lipid composition.

MLs	r_1/mM^{-1} s^{-1}	r_2/mM^{-1} s^{-1}	r_2/r_1
O	0.96	74.5	78
H	0.80	50.7	63
O-DMPC	0.90	340	378
H-DMPC	9.10	1282	140
O-DMPC-CHOL	0.80	230	288
O-DMPC-PS	0.80	798	1000
O-DOPC	0.90	630	700
H-DOPC	3.40	678	199
O-DOPC-PS	0.90	995	1000

DMPC: 1,2-dimyristoyl-*sn*-glycero-3-phosphocholine; DOPC: 1,2-dioleoyl-*sn*-glycero-3-phosphocholine; CHOL: cholesterol; PS: phosphatidylserine.

MLs composed of saturated (DMPC) or unsaturated phospholipids (DOPC), with or without CHOL or PS (negatively charged phospholipid) showed higher transverse reaction rates r_2 compared to the values obtained for SPIONs alone as a consequence of the reduction of the diffusion coefficient of water near the nanoparticles. The coating of SPIONs with lipid bilayers provided a longer interaction between the water protons and the magnetic field at the surface of the magnetic core than in absence of coating.

6. Magnetic nanoemulsions are suitable vehicles for hydrophobic drugs

NEs were chosen for their high payload, fact that favors the loading of large amounts of drugs. Therefore, multifunctional MNEs were prepared encapsulating indomethacin and SPIONs. Cytotoxicity studies were performed as described for MLs in Hela and 3T3 cellular lines. Then, the anti-inflammatory

activity of indomethacin loaded into MNEs, compared to the effect of free drug, was studied in a carrageenan-induced paw edema in rat model [26]. The height of the paw edema was measured at different times. Therefore, the study was performed with three groups of animals: A) carrageenan; B) carrageenan and indomethacin and, C) carrageenan and MNEs loaded with indomethacin. The peak of the edema was observed at 4 h for group A), and 6 h for the remaining two. The analysis of the area below the curve (Figure 9), with the Turkey-Kramer statistical test, indicated the lack of differences between groups A and B or B and C, while significant differences ($p<0.05$) were noticed between groups A and C.

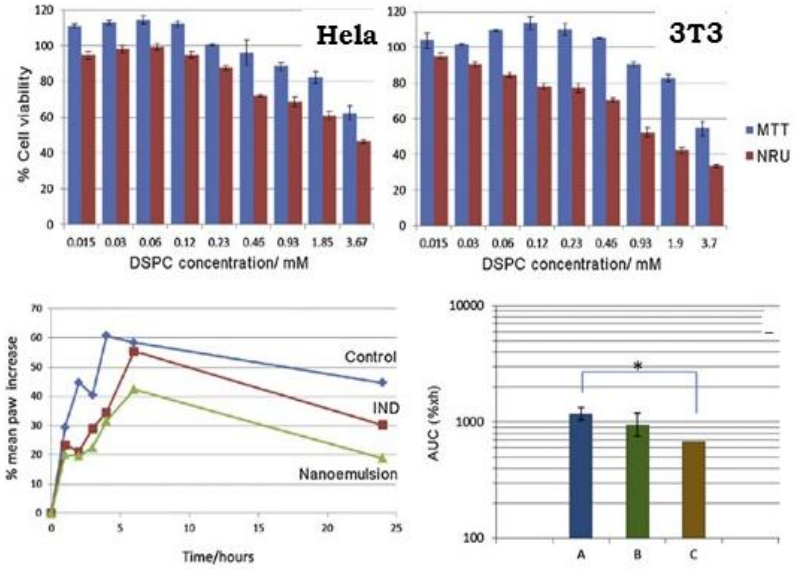

Figure 9. Top: viability of Hela and 3T3 cells after the incubation with magnetic-NEs for 24 h. Bottom left: changes in paw edema induced by carrageenan in rats at different times, after administration of saline (control), free indomethacin (IND) (2mg kg^{-1}) or indomethacin loaded MNEs (Nanoemulsion). Bottom right: area under the curve of the paw increase obtained from the data of the previous figure [26].

Ulcers in the stomachs were observed only in the group that was administered with free drug, thus confirming protective role of the NEs in reducing the drug side effects.

7. Conclusion

Stable aqueous suspensions of superparamagnetic iron oxide nanoparticles stabilized with polyethylene glycol, chitosan or alginate (ferrofluids) were successfully prepared by a co-precipitation method under mild conditions. Their incorporation into liposomes gave also stable systems that showed ability to accumulate in inflamed areas, fact that increased upon the application of an external magnetic field. Magnetoliposomes presented enhanced negative transversal relaxivity (r_2) compared to SPIONs, fact that indicates their suitability as negative contrast agents for magnetic resonance imaging. On another hand, magnetic nanoemulsions showed to be good vehicles for indomethacin with reduced side effects in comparison with the administration of the free drug. In summary, MLs and MNEs are good candidates as nanosystems for magnetic resonance imaging, for delivering hydrophobic drugs and can behave as stimuli-responsive drug delivery systems.

Acknowledgements

The authors are grateful to Dr. M. Carmen Morán for the cellular studies and to Dr. Elvira Escribano and Dr. Josep Queralt for the *in vivo* experiments.

References

1. Attama, A. A.; Charles, L. 2014, Handbook of Functional Nanomaterials. Edited by Aliofkhazraei, M., 2, 1-41.
2. Sapsford, K. E., Algar, W. R., Berti, L., Gemmill, K. B., Casey, B. J., Oh, E., Stewart, M. H.; Medintz, I. L. 2013, *Chem. Rev.*, 113, 1904.
3. Warner, S. 2004 *Scientist*, 18, 38
4. Hassanzadeh, P., Atyabi, F., Dinarvand, R., 2018, *J. Controlled Release*, 270, 260.
5. Bhise, K., Sau, S., Alsaab, H., Kashaw, S. K., Tekade, R. K., Iyer, A. K., 2017, *Ther. Deliv.*, 8, 1003.
6. Estelrich, J., Escribano, E., Queralt, J., Busquets, M. A. 2015, *Int. J.Mol. Sci*., 16, 8070.
7. Subhankar B., Kleemann, W. 2008, *J. Phys. D: Appl. Phys*., 42, 013001
8. Busquets, M. A., Espargaró, A., Sabaté, R. Estelrich, J. 2015, *Nanomaterials*, 5, 2231.
9. García-Jimeno, S., Escribano, E., Queralt, J., Estelrich, J. 2012, *Nanoscale Res. Let.*, 7, 452
10. Kalber, T.L., Ordidge, K.L, Southern, P., Loebinger, M. R., Kyrtatos, P.G., Pankhurst, Q.A., Lythgoe, M.F., Janes, S.M., 2016, *Int J Nanomedicine*, 11: 1973.
11. Atukorale, P. U., Covarrubias, G., Bauer, L., Karathanasis, E. 2017, *Adv. Drug Deliv. Rev*., 113, 141.

12. James, M. L., Gambhir, S.S., 2012, *Physiol. Rev*., 92, 897.
13. Huang, Y., He, S., Cao, W., Cai, K., Liang, X. J. 2012, *Nanoscale*, 4, 6135.
14. Martínez-González, R., Busquets, M.A., Estelrich, J. 2016, *Int. J. Mol. Sci.*, 17, 1209.
15. Laurent, S., Vander, E. L., Muller, R. N. 2013 Edited by Merbach, Andre; Helm, Lothar; Toth, Eva, Chemistry of Contrast Agents in Medical Magnetic Resonance Imaging (2nd Edition) 427-447.
16. Prasad, A. I., Parchur, A. K., Juluri, R. R., Jadhav, N., Pandey, B. N., Ningthoujam, R. S., Vatsa, R. K. 2013 *Dalton Trans*. 42, 4885.
17. Kirui, D. K., Khalidov, I., Wang, Y., Batt, C. A. 2013 *Nanomedicine* 9, 702.
18. Kiwada, H., Sato, J., Yamada, S., Kato, Y. 1986, *Chem. Pharm. Bull.*, 34, 4253
19. De Cuyper, M., Noppe, W. 1996 *J. Colloid Interf. Sci*., 182, 478
20. Sabate, R., Barnadas-Rodriguez, R., Callejas-Fernandez, J., Hidalgo-Alvarez, R. Estelrich, J. 2008, *Int. J. Pharm*., 347, 156
21. Lahiri, B. B., Ranoo, S., Zaibudeen, A. W., Philip, J. 2017, *J. Magnetism Magnetic Mat*. 441, 310.
22. Berger, P., Adelman, N. B., Beckman, K. J., Campbell, D. J., Ellis, A. B., Lisensky, G.C. 1999, *J. Chem. Ed*., 76, 943.
23. Castelló, J., Gallardo, M., Busquets, M. A., Estelrich, J. 2015, *Colloids Surf., A: Physicochem. Eng. Aspects* 468, 151.
24. Estelrich, J., Busquets, M.A., Morán, M.C. 2017, *ACS Omega* 2, 6544.
25. García-Jimeno, S., Escribano, E., Queralt, J., Estelrich, J. 2011, *Int. J. Pharm*. 405, 181.
26. Kwasigroch, B., Escribano, E., Morán, M.C., Queralt, J., Busquets, M. A., Estelrich, J. 2016, *Int. J. Pharm*., 515, 749.
27. Rodríguez-Burneo, N., Busquets, M. A., Estelrich, J. 2017, *Nanomaterials*, 7, 190.
28. Albanese, A., Tang, P.S., Chan, W.C.W. 2012, *Annu. Rev. Biomed. Eng*., 14, 1
29. Wacker, B. K., Alford, S. K., Scott, E. A., Thakur, M-D., Longmore, G. D., Elbert, D.L. 2008, Biophys J. 94, 273.
30. Koning, G.A., Schiffelers, R.M., Wauben M.H, Kok, R.J., Mastrobattista, E., Molema, G., ten Hagen T.L., Storm G. 2006, *Arthritis Rheum*. 54, 1198.
31. Dubey, P.K., Mishra, V., Jain, S., Mahor, S., Vyas, S.P. 2004, *J Drug Target*. 12: 257.